17

On the Design of a Super Wide Band Antenna

D. Tran, P. Aubry, A. Szilagyi*, I.E. Lager, O. Yarovyi and L.P. Ligthart
International Research Centre for Telecommunication and Radar, Delft University of Technology, the Netherlands
**Military Equipment and Technologies Research Agency, Romania*

1. Introduction

The adopted term *ultra wideband* (UWB) technology in 1989 by the U.S. Department of Defense, is a technology also known as impulse, baseband or carrier-free radio technology, this technology had a relatively long history, rooted deeply in the *spark-gap* experiment that Heinrich Hertz pioneered radio waves in 1886. Hertz was the first to prove experimentally that energy could be transported through space at the velocity of light by action of electric- and magnetic-waves waves, which was theoretically predicted by James Clerk Maxwell in 1873. Hertz's spark-gap apparatus with an end-loaded half-wave dipole as transmitting antenna and a resonant square loop antenna as receiver could describe as a complete UWB radio system, this famous experiment laid a fundamental concept for wireless transmission and reception of *radio-waves*, at the time more common called *Hertzian-waves* (Kraus, 1985).
Gugleilmo Marconi took Hertz's spark-gap out of the academic laboratory and successfully applied this pulse-communication to wireless telegraphy, he improved the distance between transmitter and receiver by 2 miles in 1895, 15 miles in 1897 and successful sent a Morse code of an "S" letter over the Atlantic ocean in 1901, since then the spark technology dominated the world's wireless technology with its golden period 1901-1915 (Belrose, 1995). Nevertheless, the spark gap technology development was disrupted because: a) the spectral efficiency of the signals generated by the spark-gap transmitters was low, b) as more people was trying to transmit Morse code, the interference between different transmissions were becoming so serious that receiving of the wireless telegraphy became impossible, c) research works in wireless telephony pioneered by Reginald Fessenden and others (Brodsky, 2008) had altered research interests from wideband to narrowband communications, which allowed frequency division multiplexing, offered an easy way of transmitting multiple signals in a finite bandwidth (Molisch, 2007), d) a set-back of impulse communication had been a fact when the U.S. government began banning spark transmitters in 1924 (Brodsky op cit.).
Ultra-wideband radio technology (UWB-RT) inherited a potential of extremely high rate of data communications, Claude Shannon discovered this in 1948 and derived the later-called-as Shannon-Hartley's *channel capacity laws*. This famous theoretical law however was not able to substantiate in practice until the development of the sampling oscilloscope by Hewlett-Packard in 1962, which, in accordance with the Nyquist-Shannon *sampling theorem*, was then capable to reconstruct at-that-time rather large UWB signals (Wilson, 2002).

The needs of sensors that can identify camouflaged and buried objects, and the low probability of intercept and high ranging resolution accredited from research on "time-domain electromagnetic" in the 60s, was attractive to military and radar applications, these attractions brought pulse communication back to business (Razavi et al., 2005).

UWB-RT, thus far, has been around for half a centuries but most research confined only in military applications and systems. The release of the 7.5 GHz of unlicensed spectrum by the US Federal Communications Commission (FCC, 2002) for commercial usages and applications in 2002 sparked a renewed interest in R&D of UWB-RT in industries, universities and governments. Today "ultra-wideband" usually refers UWB-RT where the electronic systems should be able to coexist with other electronic users (FCC, 2004). The UWB-RT has gained strong foothold in many applications in the areas of communications, in industries, health monitoring, law-enforcement, defense and public security, etc., The UWB-RT has established indeed as an inevitable technology in the fabric of our everyday life, however, there remains significant number of challenges for the technology to become ubiquitous, especially in the safety and security issues.

Enhanced by the decision on choosing millimeter wave-based airport security passenger screening sensors by the Transportation Security Administration, new research directives in public security domain are the search for sensors with higher channel capacity, and screening with higher resolution. To compromise both range and Doppler-resolution (Thor, 1962), sensors which support super-wideband (SWB) signaling could be the solution for the problem at hand. Super-wideband radio technology (SWB-RT) could possibly be a potential approach enables high-resolution sensing in free space and in matter including ground-penetrating radar and through-wall sensing. SWB-RT has unique advantages as compared to narrowband technology, and also comprised all UWB-RT's advanced features but with more channel capacity, higher precision and super resolution in communication, ranging and screening, respectively.

One of the challenges in the realization of SWB radio systems is the development of a suitable antenna that sustains SWB-signaling. To obtain wider bandwidth, several bandwidth enhancement techniques have been studied such as: using log periodic arrays in which the different elements are deduced from an homothetic ratio (Rahim & Gardner, 2004), introducing a capacitive coupling between the radiating element and the ground plane (Rmili & Floc'h, 2008), using microstrip-line feed and notching the ground plane (Tourette et al., 2006), using symmetrical notch in the CPW-feeding (Zhang et al., 2009), asymmetrical feeding by micro-strip line together with reduced ground plane and appropriate gap-patch distance (Karoui et al., 2010), adding T-slots for both patch and feeding strip (Rahayu et al., 2008), using cross-lot in the truncated circular patch with tapered microstrip feed line (Kshetrimayum et al., 2008). All these techniques are based on the modification of the surface current distribution to broaden the antenna's impedance bandwidth.

We report here a new SWB antenna architecture (SWBA), whose structure is purposely designed to support the functional section design approach (FSD, i.e. dividing the antenna structure into functional sections). The FSD in turn was utilized to accelerate the bandwidth optimization process; the SWBA and FSD together have conclusively enabled the designer to obtain antennas with SWB performances by optimization of just a most-significant-parameter. It is noted here that in our SWB antenna, hereafter-named prototype 4,

modifications were made at not only the feed-section but also the transition section and the radiation-section as well.
Anticipating and combining of all the advantages of its predecessors (prototypes 1, 2, 3), our new SWP-prototype 4 has been designed, fabricated and evaluated. Measurement results revealed that its SWP-performances are superior to other SWP-radiators reported in open-literature.
It is also worth noting here that our SWB antenna was one of the successful results of the long cooperation between the International Research Centre for Tele-communications and Radar (IRCTR) in the Netherlands and the Military Equipment and Technologies Research Agency (METRA) in Romania.
This chapter is organized as follow: First, in §2 we discussed briefly the wire-version-antennas that all planar UWB and SWB antennas were derived thereof, the concepts of quasi-electric and quasi-magnetic for planar antennas are typically discussed, also definitions pertaining to qualitatively expressing the SWB antenna's impedance bandwidth were considered. In §3, the SWBA and the FSD are proposed and discussed. In §4, we briefly examine the performance of radiator prototype 1 as a "proof of concept" and provide a methodological procedure for simplifying the multivariate optimization (MVO) process, which were intensively used in the design of other prototypes 2, 3, 4, also parametric investigations and numerical simulations of the proposed SWB radiator are shown in this section. Technical issues related to the practical consideration of the design and fabrication are discussed in §5. Measurements of impedance bandwidth, reception patterns and pulse characteristics in both frequency- and time-domain are reported in §6. Acknowledgements are expressed in §7, and final conclusions are summarized in §8.

2. Fundamentals

In designing mw- and mm-wave antennas and components, planar technology offered numerous advantages in comparison to wire- and waveguide-technologies, such as planar, light weight, small volume, low profile, low cost, compatible with integrated- or with active-circuits, easy integrate into passive or active phased arrays and communication systems.
The planar technology facilitates the designers much flexibility in creating a myriad of different UWB and SWB antennas, the architectures of these antennas may different but their topology mainly resembles the traditional wire-version of monopole- or dipole-antennas. The nomenclatural names of planar antennas are confusingly taken over from the wire-version with similar topology. Topological similarities may support such borrowed name, nevertheless it is incorrect—as discussed in the next subsections—regarding to electromagnetic-properties point of view. To avoid such inconsistent idealizations new names and definitions, which support both topological and electromagnetic point of views, will be introduced in this section. We briefly start with recalling the traditional wire-version dipole and monopole antennas in §2.1, then the correct nomenclatures—for the planar-version magnetic and electric antennas—are introduced in §2.2, and end with their similarities: quasi-electric and quasi-magnetic antennas in §2.3.

2.1 Dipole and Monopole Antennas

The *Dipole* antenna is one of the oldest radiators with theoretical expressions for the radiation fields being readily available (Balanis, 1997, p.135). The shapes of their radiation

patterns are also well-known [ibis., p.154]. The antenna first used by Hertz in his early RF experiments in the late 19th century, as an example, was a half-wave dipole (Krauss, op. cit.) and the shapes of its 3D-radiation pattern had a similar appearance to a full-doughnut or figure-eight (Balanis op. cit. p.163).
The *Monopole* antenna is formed by replacing one half of the dipole antenna with the ground plane, when the ground plane is large enough the monopole behaves like the dipole, except that its radiation pattern is just one half of the dipole, its gain is twice, while its length is one half of the dipole.
Magnetic dipole and *electric dipole* are standardized and well documented in [IEEE STD 145-1983, p.11-16]. The terms magnetic antenna and electric antenna were logically defined but occasionally used in literature, the first term used to describe radiators which posses radiation properties resembling those of thin wire loop (Balanis, op. cit., p.217), while the second is for those resembling of thin wire linear antennas.

2.2 Electric and Magnetic Antennas

Planar UWB and SWB antennas which geometrically resemble its counterpart (wire)-monopole antennas are widely called monopole. However, this topological naming for the planar radiators is incorrect and confused, because the radiation pattern of all the so-called (planar)-monopole antennas have not the shaped of the monopole but of the dipole antenna i.e., having the shape of the full-doughnut.
To avoid ambiguities, formal definitions for planar antennas are hereafter provided.
The definitions planar-magnetic antenna and planar-electric antenna were constructed by means of an analogy to the wire-loop antenna and the wire-electric dipole which are documented in (IEEE Std, op. cit.; Schantz et al., 2003, 2004; and Tanyer et al. 2009a), to keep this chapter self-content and avoid cross-reference, we summarize them here:
As a first step, let the *base plane* $\boldsymbol{B}$, be the plane comprises the antenna's effective radiating/receiving aperture, and let $\mathbf{n}$ be the unit normal vector to this plane, with reference to figure 1, $\boldsymbol{B}$ can be assimilated into xOy, while $\mathbf{n} = \mathbf{i}_z$.
Assume that the field has a transverse electromagnetic (TEM) distribution propagating along the base plane. Then the following cases can be distinguished:

1. In the case when the base plane *magnetic field* $\mathbf{H}(\mathbf{r})$, with $\mathbf{r} \in \boldsymbol{B}$, is directed along $\mathbf{n}$, the radiator is referred as *magnetic antenna*.
2. In the case when the base plane *electric field* $\mathbf{E}(\mathbf{r})$, with $\mathbf{r} \in \boldsymbol{B}$, is directed along $\mathbf{n}$,the radiator is referred as *electric antenna*.

The above definitions are strictly applied to structures that support propagating-and-non-rezo TEM- field distributions only, so that the waveguide case is automatically excluded by this TEM regard.
We note here that the above definition have not taken in to account the diffraction effects at the edges/vertexes/corners of the metallic/dielectric material that constituent the transmitting/receiving aperture.

2.3 Quasi-Electric and Quasi-Magnetic Antennas

Most of the cases, particularly in planar antenna configuration, the topology of the radiating apertures may prevent the above-indicated conditions from being rigorously satisfied. Even in such cases, either one or the other of the two situations may prevail, thus correctly

determine the type of the antenna. For instant, a radiator for which the magnetic field strength **H**(**r**) or the electric field strength **E**(**r**) is parallel to **n** over most of the effective aperture will be denoted as *quasi-magnetic* antenna, or *quasi-electric* antenna, respectively.
Obviously, planar antennas fed by microstrip-line or co-planar-waveguide can be classified as quasi-electric or quasi-magnetic antennas, respectively.
As will be demonstrated hereby, our prototypes fall in the class of quasi-magnetic antennas, whilst for all patch antennas fed by micro-strip line, as an example, the RAD-NAV antenna (Tran et al., 2010) belongs to the class of quasi-electric antennas.

2.4 Bandwidth Definitions

There are several definitions of bandwidth circulated among our antennas and propagation society; those frequently met are octave-, decade-, ratio-, fractional-, percent-, and ratio-bandwidths. The two definitions, that most frequently used, are the percent bandwidth and the ratio bandwidth. They are defined respectively as follows:

$$B_P = 100\% \times BW / f_C \tag{1}$$

$$B_R = BW / f_L \tag{2}$$

Where:

f_H, f_L are the maximum and minimum frequency at -10 dB, respectively.
BW is the nominal bandwidth defined by $BW = f_H - f_L$
f_C is the central frequency defined by $f_C = (f_H + f_L)/2$
B_P is the percent bandwidth and,
B_R is the ratio bandwidth, commonly noted as B_R = R : 1, where R is the ratio defined as R= f_H/f_L

The *percent bandwidth* (1) has originally been used to describe the narrow-bandwidth of conventional antennas and microwave-devices. Its usage is quite popular and often considered as a standard in many textbooks, nevertheless, it is mathematically not a solid definition because it possesses a defect when f_L approaching zero. For example, suppose that the nominal bandwidth of antennas #1 is 2GHz (0-2GHz), and antenna #2 is 20GHz (0-20GHz). It is clearly that the nominal bandwidth BW of the second antenna is 10 times wider than the first one; however, formula (1) indicates that both antennas have the same percent bandwidth. Another weak point is the percent bandwidth of formula (1) is always less than or equal to 200% irrespective of how wide the antenna's nominal bandwidth was. Note also that formula (1) is often mistakenly called as *fractional bandwidth*, indeed the formula (1) consolidates its meaning "fractional bandwidth" only when the factor 100% is removed.
Alternatively, the *ratio bandwidth* (2) can also be used for expressing the bandwidth of UWB and SWB antennas and devices. The defect at zero- frequency point still lurks there but the 200%-limit is lifted. The use of the ratio bandwidth is more adequate to envision the wideband characteristics of devices under investigation. We choose for the second formula (2) for describing the bandwidth for the SWB-prototype discussed in this chapter.
How to choose two formulas, although no official consent however, the first formula is often used for cases that the bandwidths are less than 100%, whilst the second is for UWB and SWB antennas/devices.

Traditional communications systems typically used signals having a percent bandwidth of less than 1%, while standard CDMA has an approximately of 2%. Early definition in the radar and communications fields considered signals with percent bandwidth of 25% or greater (measured at the *-3 dB points*) to be ultra-wideband. The recent FCC regulations (IEEE Std, 2004), which will be used as a standard throughout this text, defined UWB devices/signals as having an nominal bandwidth which exceeds 500 MHz or percent bandwidth of over 20%, measured at *-10 dB points*.
The term SWB has been often used to indicate bandwidth, which is greater than a decade bandwidth. Since the percent bandwidth confused and failed to envision the SWB property adequately as discussed in §2.4, the "ratio bandwidth" is more suitable and often be used for describing bandwidth of 10:1 or larger, we adopt this convention throughout this report.

3. Antenna Topology, Architecture and the FSD Methodology

Since the release of the license-free band and the regulation of the emission spectra by the FCC in 2002, a myriad of UWB antennas have been created and invented by both industry and academia, most of them are limited to the FCC-band, this 7.5GHz bandwidth corresponds to a moderately short pulse in order of nanoseconds, these short pulses are good enough for high capacity communication, accurate ranging and imaging but not enough for the more stringent needs of precise localization, high resolution screening, sensitive sensing. To satisfy such stringent requirements, challenges are placed on the design of sensors that support signaling of extreme short pulse in the order of hundreds of picoseconds or less. Sensors in the terahertz region support such short pulse and unarguably provide sharpest images, nonetheless the detection range is too short and the sensors are very costly. Note that in the terahertz region, a radiator with only 5% is capable to support, for example, a Gaussian pulse of 20 Ps (assumed unity time bandwidth product), while in the RF-region one must have a SWB radiator of over 11:1 (or 167%, by a lowest frequency of 5GHz) for signaling such a short pulse.
There existed broadside and end-fire UWB antennas with different topologies, which comprised of many configurations are available in open literature. The pattern stability of several antenna's topologies and architectures had been thoroughly investigated and reported by (Messey, 2007, p.163-196). It seemed that there was no broadside antenna architecture could exhibit stable patterns within a bandwidth wider than 10 GHz, and most of them are UWB-radiators with ratio bandwidth much less than 10 : 1.
We propose here an SWB antenna architecture which possessed not only SWB bandwidth lager than 10:1 but also exhibited a much stable patterns in its SWB bandwidth than all those which have been studied and reviewed by (Messey, op. cit.). The SWB prototype 4, and all other prototypes reported in this chapter had been designed, fabricated and evaluated at our IRCTR.
The SWB radiator reports in this chapter, was indeed a revolutionary improved version from IRCTR's previous developed prototypes. All the developed prototypes, shown together in fig. 4, shared the same topology and architecture as depicted in Fig. 1a. The kernel of this topology is its simplicity, and the essence of the antenna's architecture is the logicalness of dividing the antenna into functional sections that enables simplifying the MVO process into a sequence of single-variable optimization (SVO) one.

The merits of the topology, architecture and logical functional blocks, and optimization process will be discussed in §3.1, 3.2 and 3.3, respectively.

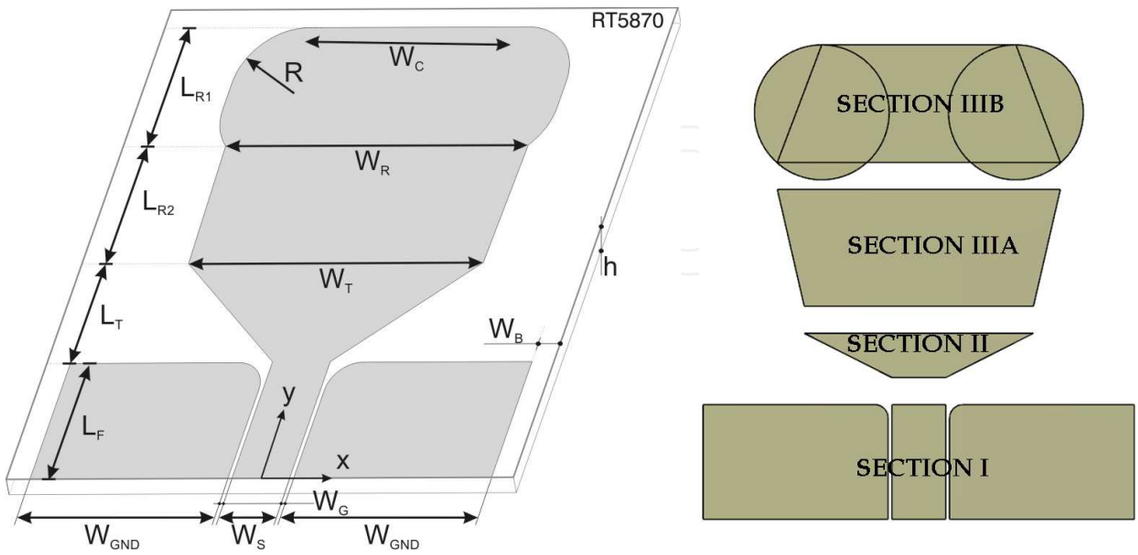

Fig. 1. Proposed configuration: a) Architecture and parameters, b) logical functional sections.

The original antenna topology and architecture of prototype 1 leaved many flexible possibilities for adjusting parameters or scaling dimensions to meet new requirements or applications without much entangled in complicated MVO process. These possibilities have been exploited to double the antenna's bandwidth of prototype 1 (Tran et al, 2007) from 2:1 to 4:1 by (Tanyer et al., 2009a), and further broaden to 9:1 (Tanyer et al., 2009b), and scaled down to the FCC-band for IR-applications (Tanyer et al., 2010).

The prototype 4 is a proof of concept in proving viability of the design of radiators, which are capable of supporting such extreme short-pulse in RF/mw-region. The proposed antenna's topology, architecture and the FSD approach, as will be discussed in subsequence sections, were objectively aimed at two main goals:

- Choosing an antenna topology whose shape is kept simple regarding ease of fabrication, prevent diffractions, easy to scale up/down to meet designer's requirements in size and performance (§3.1).
- Creating an architecture that providing a basis platform for implementing the "FSD approach", and deploying the conceptual "thumb-rules" for effective simplifying the MVO process in to SVO, a much simpler one (§3.2).

3.1 Antenna Topology

The starting point in the design of the SWB antenna reports in this section is mainly credited to the original radiator (Tran et al., op. cit.), whose topology is planar, as sketched in Fig. 1a, with structural topology comprised of following stack-ups:

- Single dielectric layer to provide structural rigidity.
- CPW feeding structure on top of the structure.
- An antenna patch is directly connected to the CPW-feeding, so that they together formed a single planar pattern run on top of the structure.

The CPW feeding structure has been chosen because of it well-behaved properties: such as negligible radiation, low loss, the effective dielectric is constant over a sustained wide frequency range, where the later property is more suitable for super-wide-band feeding a SWB-radiator than the micro-strip line (Simons, 2001).

3.2 Antenna Architecture and the FSD Approach

In antenna design if dimensions are unconstrained and by a proper design, antenna will behave as a high pass filter, and if its dimensions are physically large enough then all frequencies will pass through. Research of published papers over UWB and SWB antennas reveals that most of the UWB and SWB antennas had a considerable larger size, mostly lager than $\lambda_L/2$ of the lowest frequency f_L, and on broadening the bandwidth, a first option, was to resort to stochastic optimization methods, nevertheless, these methods are known for carrying extremely high computational load.

A more feasible alternative approach was provided by the critical analysis of the relation ship between the geometrical parameters and the physics of the problem at hand. The FSD approach was intentionally created in such a way that the overall dimensions are constrained, kept small and the process of optimization can also be simplified.

The logical architecture together with its parameter and FSD-blocks are sketched in fig. 1.

The FSD approach follows the bottom-up strategy, i.e.:

- Starting from the feed section—its CPW feed supports the required impedance bandwidth for SWB signaling.
- Then to the internal transition section—this section is intentionally inserted between the feed and the patch for the purpose of impedance matching, its shape was logically chosen so that it able to serve the design-properties: resonance shifting, impedance matching, and also enable parameter to serve as independent optimized parameter.
- In addition to the radiating section, we divided it in to two sub-sections, which are the patch section and the external transition. The patch section creates an extra degree of freedom to ease the optimization process, and the radiating section provides parameter for shaping radiation patterns. Two round areas had been added to the top corners of the patch for the purpose of 1) diminishing of diffraction at the antenna's top vertices (deformation of sharp corner in to circular edge) and, 2) controlling and retaining the shaped of the radiation patterns at high frequency band of the spectrum, and, 3) subduing the number of parameters to accelerate the optimization process. These four sections are orderly numerated as I, II, IIIA, and IIIB in Fig. 1b.

In summary, the FSD approach assumes the following steps:

- Keep the antenna's overall dimension small and fixed;
- Start orderly from section I, II, IIIA and IIIB (this bottom-up strategy prefers matching impedance bandwidth in prior of pattern bandwidth);
- Separate and understand the role of each section;
- Identify the parameters associate with that section; select the parameter that predominantly influences the function of that section.
- Isolate the effect of that parameter so that an optimization only on that parameter can be undergone, without affecting too much the performance of other sections.

Based on the FSD approach the prototype 1 was first designed and evaluated. Its designed parameters are used as start values for the optimization process of all the later prototypes.

Four prototypes (1, 2, 3, 4 shown in fig. 4) were successful designed and evaluated, the prototype 4 proved to be a radiator which is superior to the others in that both of its impedance bandwidth and radiation pattern are SWB-sustainable.

4. Parameter identification and optimizations

The prototype 1, elaborated by (Tran et al. 2007), formed a basis for the designs of the later prototypes. Its 10GHz impedance bandwidth and designed parameters are plotted in fig. 5 and listed in table 1, respectively. For the detailed works and the measurement results, the reader should refer to (Tran et al., op. cit). The other prototypes all took the designed parameters of prototype 1 as start-values, and used the FSD to identify the significant parameter for its SVO process of bandwidth broadening.

The prototype 2 was obtained by taking the start values of the prototype 1, and using FSD to identify the L_T as its significant parameter for SVO process. The resulting designed parameters and the impedance bandwidth are listed in 2nd column of table 1, and Fig. 5, respectively. The SVO demonstrated the solidity of the FSD approach that the bandwidth can be doubled (from 10GH to 20 GHz) by optimization of just a single parameter L_T. For details of the elaborated work, please refer to (Tanyer et al., 2009a, op cit.)

By keeping L_T fixed, the prototype 3 is obtained by optimizing the lower part of the radiation section which comprised of two parameters L_{R2} and W_T, the first make the total length of the radiator shorter (thus affects the higher frequency), whist the second parameter provide an better match (i.e., lower reflection coefficient). By doing two SVO sequentially (first with parameters L_{R2}, then W_T) we again doubled the nominal BW (form 20GHz to 45GHz), in term of ratio bandwidth it is of B_R = 9:1 as shown in Fig. 5. The resulting parameters are listed in column 3rd table1. Further details of measurements and other properties of this prototype 3, are detailed in (Tanyer et al., 2009b, op. cit).

Prototype 4 is obtained by the combined optimization of the FSD-indentified parameters W_T and W_C, By keeping the optimized parameters of the previous optimization steps (L_T of prototype 3, all others of prototype 1) fixed, and doing 2 SVO sequences, we obtain the SWB impedance bandwidth of B_R greater than 30:1, the result is plotted in Fig. 2. The design parameters are listed in table 1. We noted here that by controlling radii-separation distance W_C we are able to keep the radiation pattern of this prototype less distorted till 50GHz as shown in Fig. 3.

The created parameters, their functions, their effects and their usages are discussed in greater details in the next sub-sections. The FSD is detailed in §4.1-4.3, the resulted SWB-performances are given in §4.4 and in §4.5 the optimizations of all the prototypes are discussed in details.

4.1 Section I: The feed section

Planar antennas and arrays have been used for micro-wave and millimeter-wave applications for decades, especially in mobile communications where system design requires low profile, lightweight, and high directivity. The two most used feeding methods

are micro-strip line (MS) and coplanar waveguide (CPW), they both carried signal excellently in narrow-band and UWB antennas and devices. Many planar antenna arrays have been designed by using MS, however, until recently, only a few works so far have used CPW to feed the array. The CPW has gained increasing popularity in recent years, since it has several advantages over the MS, such as low radiation losses, less dispersion, easier integration with solid-state active devices, and the possibility of connecting series and shunt elements, and suitable for SMD-technology, also for SWB- antennas/devices CPW feeding provides better match and performs better than the MS line (Simons, 2001).
In search for the SWB radiator, both radiator and the feed must be super wide band. Since the SWB-signal first must able to pass through the feeding-line before reaching the antenna, obviously that the feed must be considered first in advance of other sections, we conduct the work with bottom-up approach, i.e., the feed is consider first, because if the feeding mechanism fail to be SWB, then there is no SWB radiator exists no matter how good the radiator will be. The coplanar waveguide is the first choice for feeding the signal to the radiator, because the CPW's effective dielectric is constant, (this property is a key feature in wide band matching the antenna), over a wider BW than micro-strip line, another advantage is, in contrast with MS line, one of the parameter pair (W_S, W_G) can be varied in size and shape, whilst the other is correspondingly changes to keep the characteristic impedance stays unchanged, furthermore CPW is low-loss, and the signal width can be chosen width enough to support characteristic impedance from 30Ohm and higher (Simons, 2001, p.52),
The CPW would be a better choice for SWB-feeding because of it considered features, summarized as follows:

- SWB behavior: the effective dielectric constant is almost independent of frequency (Simon op cit.), this feature is a priori condition for super wide band feeding and matching.
- Dimensional flexibility: the width of the signal line, and hence the corresponding gaps, can be freely designed to accordingly support the physical dimension of the transition region and the antenna.
- The dielectric thickness exerts negligible weight on the economy of the CPW-impedance.

4.2 Section II: The Tapered Transition

The tapered transition has been inserted between the CPW-feed and the radiating patch, this section responsible for a smooth transition between the feed and the antenna, and because the current distribution is denser in this region than the others, this property indicated that this section must have strongest influence in matching the impedance bandwidth. This section has two parameters (L_T, W_T), which are described in details in §4.2.1 and §4.2.2 below

4.2.1 The Internal Transition Length L_T

The length L_T of the tapered transition (section II) is responsible for the smooth transition between the feed and antenna, and proved to be the most sensitive parameter in the design of our prototypes. Anticipation from the theory and design of micro-strip antenna (MSA), it is well-known that the length of the MSA determines the resonance frequency (by lengthen or shorten this parameter, one can shift the resonance frequency to lower or higher band, respectively).

The antenna's resonance is affected by its length, this length is composed by $L_T + L_{R1} + L_{R2}$, when this composed length is changed, and the resonance will presumably change accordingly.
It is observed, from the results plotted in Fig. 5, that when L_T is longer the resonance will shift to lower frequency (as shown by prototype 1, L_T = 6.4, Fig. 5), and when L_T is shorter the radiator's resonance will shift to higher frequency (prototype 2, L_T = 1.64, Fig. 5)

4.2.2 The Internal Transition Width W_T

The width W_T of the taper transition section (section II), is also a "share-parameter" with lower radiating section (section IIIA); this width provides, as similar role as the width in microstrip patch antenna, a fine-tune mechanism for impedance matching as its nominal value varies. This enhanced matching mechanism are numerically demonstrated with the reflection coefficients of the prototypes 3 and 4 as plotted in Fig. 5, in which they shown a lower reflection coefficient, i.e., a better match.

4.3 Section III: The radiation section

This section comprise of six parameters L_{R1}, L_{R2}, W_T, W_R, W_C, and R_C, in which W_T is the share parameter described in §4.2.2, we divided this section into sub-sections IIA and IIB as sectioned in Fig. 1b. The parameter set of the internal sub-section (IIIA) and the external parameter sub-section (IIIB) are {W_T, W_R, L_{R2}} and {W_R, L_{R1}, W_C, R_C}, respectively.

4.3.1 The Internal Radiating Matching Section

Two parameters, which identified to be key player for this subsection, are {W_T, L_{R2}} (the W_R is not touched because it is share parameter of these two sub-sections), by first optimize the width parameter W_T, and by keeping this optimized parameter fixed, and continuing to optimize the other parameter L_{R2}. By this token, (Tanyer et al., 2009b, op cit.) obtained a huge enhancement in ratio bandwidth reported as 9:1. The design parameters are listed in table.1, the result is plotted in fig. 5. More detailed works and measurement results, the reader should refer to (Tanyer et al., op cit.).

4.3.2 The External Radiating Transition Section

This sub-section was often neglected by the designers due to the fact that the current distribution is weak along the edges of this section. However, we observed that it plays an important role in maintaining the shape of radiation pattern in a wide range of frequencies, as will be numerically proved in §4.4

The sub-section IIIB consists of a set of parameters {W_R, L_{R1}, W_C, R_C}; W_R is a share parameter so we keep it intact. From fig. 1 it is seen that W_{R1} is suppressed and covered by varying the radii-distance W_C, we can also single L_{R1} out because it contribution to the length of the radiator can already be economized by L_T and L_{R2}, so W_C is the only parameter left that we may use to fine-tune the radiator for both SWB performance and radiation pattern characteristics. Prototype 4 utilized this philosophy by varying L_{R2} (instead of L_{R1}) and W_C to obtain the super wideband performance plotted in Fig. 2. It is observed that variation of W_C had no significant impact on reflection coefficient (current distribution along the antenna

circle edges are rather week compared with those close to the tapering transition region). Nevertheless, by properly controlling W_C we are able to maintain the usable shape of the radiation patterns up to 50 GHz as shown in Fig. 3. So, W_C is clearly to be the parameter to control the interference of the edge/corner scattering and diffraction of the radiator. In transforming the vertex-diffraction to edge-diffraction, we advocate the use of circular shape; nevertheless, other researchers suggested the shapes (elliptical, football cape, etc.). To answer the question which shape would serve best, we need a further in depth study about all possible pattern sensitive shapes before providing a final conclusive appraisal.

4.4 The prototype 4 and its Super Wide Band Performances

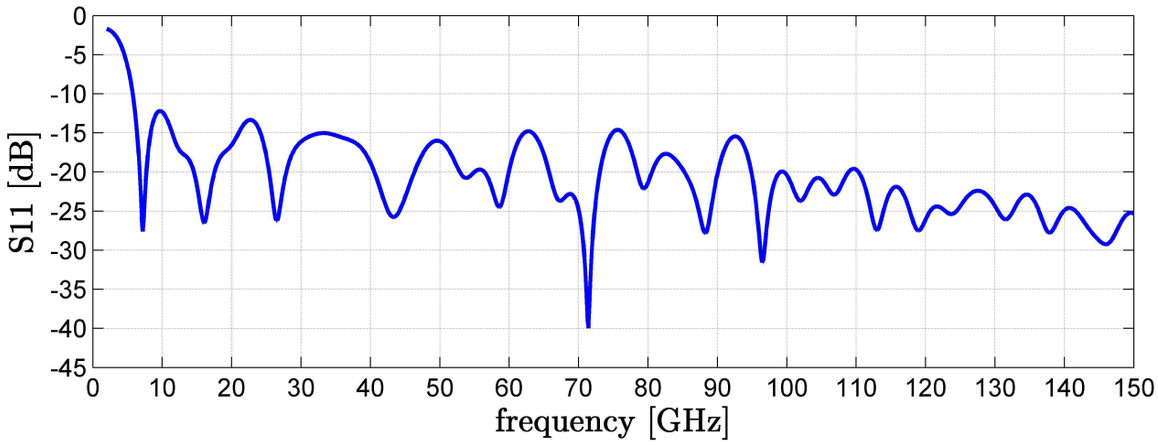

Fig. 2. Super wide band performance of the proposed prototype 4.

Fig. 2 shows the simulated result of the magnitude of the reflection coefficient of our SWB prototype 4. We computed and shown here only up to 150GHz. By close inspection of the reflection coefficient, the reader could observe that the prototype 4 shows a trend and exhibits the behavior of an all-high-pass antenna; its impedance bandwidth could be much wider than shown here.

The numerical results were computed with the following practical assumptions:

- The relative dielectric constant and the loss are assumed constant over the computational bandwidth.
- The commercial Duroid RT5870 high frequency laminated material we used, in deed could practically support up to 77 GHz only (Huang, 2008, p.64); beyond this frequency we may have to look for other dielectric material.

Figure 3 shows the simulated 3D radiation patterns of prototypes 4; the plot indicated that the radiator exhibits a super wide band pattern characteristics, the usable spherical patterns are sustained in a bandwidth wider than 10:1. The SWB properties displayed in fig. 2 and fig. 3 shown that prototype 4 is a true SWB radiator in both impedance and radiation aspects, and its SWB-behavior is superior to antennas reviewed by (Massey, 2007, pp. 163-196). We emphasize here that this radiator is termed as quasi-magnetic antenna, because it is clearly seen that this antenna possessed radiation patterns similar to that of a dipole,

therefore calling it monopole reflects wrongly the EM-characteristics that it possesses and exhibits.

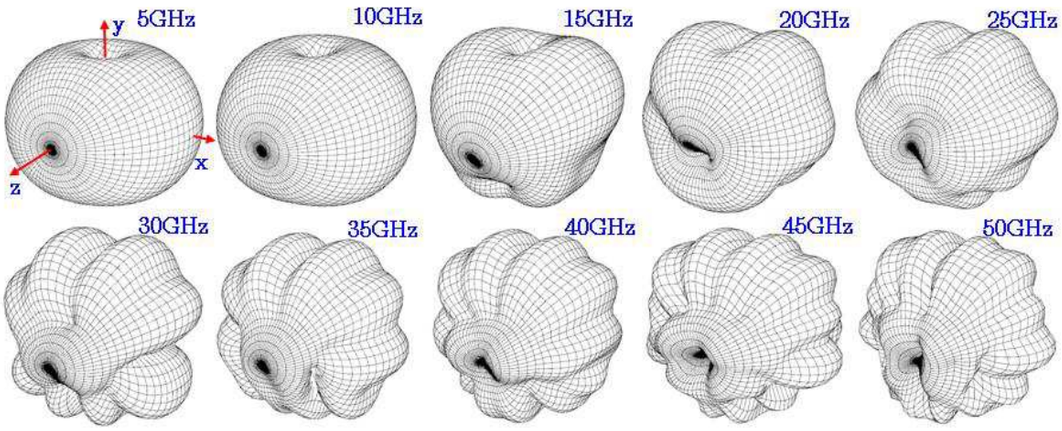

Fig. 3. Complete spectra of 3D-farfield co-polar radiation patterns from 5 to 50 GHz with increment step of 5GHz.

4.5 Optimization Process and Development of Prototypes

Although the proposed topology and architecture is simple, however with a total of 14 parameters it would be an impossible task for the multivariate optimization process.
This section reports in details of how to delimit the variables and how to reduce the number of variables for simplifying the MVO process to a SVO one. In addition, some pragmatic rules are also given for identifying the key parameters, and for weighting the priority of those parameters in the sequentially SVO processes.
To keep the optimization process controllable en less entangled in multivariate-optimization process, efforts have been done in the following steps:

Step 1—Topology and architecture: this step is important in that it had to form a basis for the FSD, and had to keep the antenna topology as simple as possible, but not simplest as (Al Sharkawy et al., 2004), Although all efforts has been carried out to ensure a minimum amount of the created parameters, the structure (fig. 1a) still have a considerable set of parameters { ε_r, h, t; L_F, W_S, W_{GND}, W_G; L_T, W_T; L_{R2}, W_R; L_{R1}, W_C, R }.

Step 2—The FSD: dividing the radiator into sections depending on their main function. Inspection of the radiator's current distribution and the radiator's topology shown in fig. 1a revealed that the radiator could presumably be divided into functional sections as depicted in fig. 1b. The analyzing and optimizing process are conducted following the bottom-up approach that always started from the feed (section I) and ended at the last radiation-section (section III.B). The analysis, optimization and development of the prototypes all should start and avoid as much as possible the *share-parameters* between sections (W_T, W_R); if impasse is met then, as a thumb-rule, the section on top has priority on taking the share parameter.

Step 3—Excluding of fixed parameters: The numbers of parameters of the radiator have been reduced by singling out the non-optimizable parameters. The first three material-parameters { ε_r, h, t}, because their nominal values were already fixed by the manufacturers,

are not quite suitable for optimization process as continuous-parameters, so the parameters of the feed section (section I) are kept fixed and excluded in the optimization process.

Step 4— Setting boundaries: in order to accelerate the optimization process and avoiding the problem of unbounded optimization, we put geometrical restrictions on the total width ($2W_{GND} + 2W_G + W_S$) and length ($L_F + L_T + L_{R2} + L_{R1}$) of the antennas fixed to $\lambda_b/2$, where λ_b is wavelength at the design-frequency, and force all the internal parameters and their combination to be constrained inside this antenna's boundary $\lambda_b/2$.

Step 5—Reduction of parameters: in this step, we did further reduction of the number of parameters involved. Exploiting the fact that the feed-section's parameters have no significant added values to the total performance once its optimum values are founded, and the following prior measures have been set, 1) for impedance-matching it is fixedly set to 50 Ω and, 2) for field-matching the impedance-parameter-pair (W_S, W_G) has been chosen such that it is wide enough to support the currents to separately flow along the edges of the signal line W_S, and the feed length L_F must be long enough to support the transformation from coax's TEM to quasi-TEM of the CPW line, so the feed's parameters can ruled out for optimization, and set to be fixed with values as listed in table.1.

Step 6—Start values: This step initiated the start values for the set of parameter listed in step 1. The initialization of the start values was elaborately detailed in (Tran et al., 2007). Prototype 1 (Fig. 4) with the start values as listed in table.1, obtained a BW of 10GHz (fig. 5). Detailed discussions and simulated, measured results can be found in (Tran et al., op. cit.).

Step 7—Simplified process: The 7th step is the simplification of the optimization process by breaking the MVO process down into series of SVO one. It was observed that the current intensity is mainly distributed along the edges of the transition region, this suggested that : a) small variation of the transition parameter in this section (L_T, W_T) would have a strong influence on the flow of the signal current and hence play a large impact on the impedance bandwidth, and exploiting the fact, as similarly in microstrip antenna, that b) the length of the radiator defines the *shifting-property* of the resonance, whilst c) the width of the radiator effectuates the *matching-property*, and d) another *independent-property* is that they can be separately optimized.
So by keeping W_T, the share-parameter between sections II and III.A (fig. 1b), fixed and took just a single-variable-optimization (L_T), the impedance bandwidth was double to 20GHz as obtained by prototype 2, which is plotted in fig. 5. The parameters of prototype 2 are listed in table.1, more details of the electromagnetic properties and measurements regarding the performances of this prototype can be found in (Tanyer et al., op. cit.).

Step 8—BW enhancement: Prototype 3 (fig. 4) was obtained by analyzing and optimization the lower part of radiation section IIIA (fig. 1b). This section has three parameters (W_T, L_{R2}, W_R); first, following the rules discussed in step 2 we left out the parameter W_R since it is the share-parameter between section IIIA and IIIB; next, in order to avoid multivariate-optimization, anticipating the shifting-property and matching-properties discussed as (b) and (c), respectively, in step 7; then two SVO sweepings were carried out, first W_T (property c) and then L_{R1}(property b); the order of W_T or L_{R1} can be chosen freely according to

independent-property (d, in step 7). The design parameters of prototype 3 are listed in table.1 in which the parameters of the previous optimized prototype are kept fixed, only the two parameters (W_T and L_{R1}) belonged to section IIIA are investigated and optimized.

Step 9: The design of prototype 4 is aimed at two SWB-compliances: 1) SWB impedance bandwidth, and 2) SWB radiation pattern. The radiation section consists of the following set of parameters (W_T; L_{R2}, W_R; L_{R1}, W_C, R), the length parameters of this set can be keep fixed, because L_{R2} and L_{R1} are resonance-shifting parameters, and the antenna architecture allows us to use other length of the antenna to control the resonance, this was already done by L_T of the lower section, so these two parameters can be singled out of the optimization process; the share parameter W_R can also be neglected because it matching-property is covered by the set {W_C, R}, so by keeping R fixed the parameter set of section III was left with only two parameters left {W_C, W_T}. The procedure followed: fist, keeping the parameters of prototype 1 with the optimized L_T = 1.64mm, then two SVOs were carried out first for W_T and then W_C. The reason that W_T was chosen first is twofold, 1) W_T is more sensitive on matching because the current distribution is denser at the lower part, 2) W_C is the share parameter that mainly located in section IIIA where the matching effect is week, and it is purposely inserted to control the radiation patterns in stead of wideband matching the radiator. The optimized parameters of prototype 4 are listed in table.1. The impedance bandwidth of the prototype 4 is plotted in fig. 2, and fig. 5; also, its SWB radiation patterns were in fig. 3.

4.6 Comparison of the prototypes

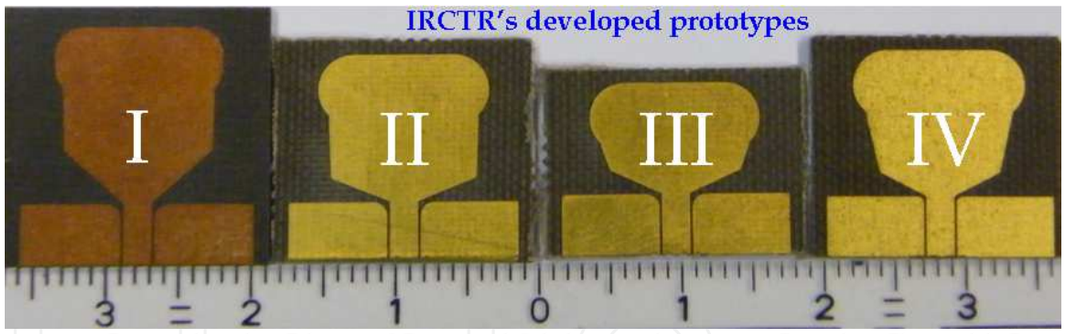

Fig. 4. Prototypes developed at IRCTR, resulted design dimensions are listed in table 1.

Prototypes 1, 2, 3, 4 have been design, fabricated, measured and evaluated, photographs of them are shown in fig 4. At first sign, they seemingly looked different, however they all shared the same topology and architecture as depicted in fig. 1a, only one or two parameters is slightly changed to obtained difference desired performances. For comparison, their correspond impedance bandwidths are plotted together in figure 5. The impedance bandwidth enhancement is improved from 10 GHz, to 20 GHz, 40 GHz and beyond 150 GHz as shown by fig. 5 and fig. 2

The design parameters of prototype 4 and all other prototypes are listed in table.1, so that, the reader, could independently recheck, or reproduce them without much difficulty.

These are results of the FSD methodology and SVO steps described in previous sub-section (§4.4). Note that the SVO should be carried out orderly by A, B and C. (bold and capitalized in table.1), A is dedicated as the first to be optimized, keep that optimized parameter fixed,

and goes on with B, then continue with C. For example, the prototype 4, (A) first fixing the taper's height L_{R2} to 4.335mm, then (B) optimizing the taper width W_T, and then (C) adjust the W_C for the radiation-characteristics. The optimized results showed an SWB impedance bandwidth of at least over 150GHz. In fact the result of prototype 4 (with parameters listed in column 4 of Table.1) shown the downtrend of reflection coefficient for increasing frequency (Fig. 2), we expect that prototype 4 will well-behave beyond 150GHz as well.

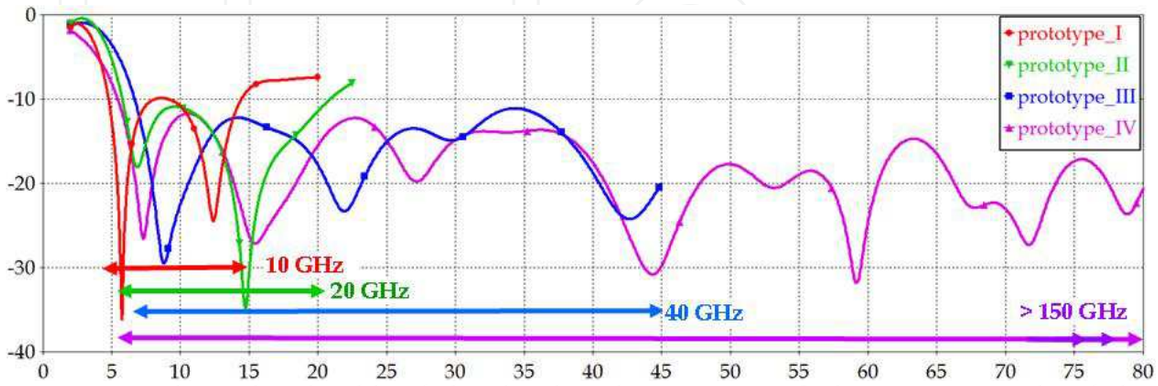

Fig. 5. Impedance bandwidth of the developed prototypes. Ordinate: magnitude of the reflection coefficient [dB]; Abscissa: frequency [GHz].

Parameter (mm)	**Prototype 1**	**Prototype 2**	**Prototype 3**	**Prototype 4**	**Description**
L_F	4.25	4.25	4.25	4.25	Length of the feed section
R_F	0.5	0.5	0.5	0.5	Blending radius in the feed section
W_{GND}	6.86	6.86	6.86	6.86	Width of the ground
W_S	2	2	2	2	Width of the signal line
W_G	0.14	0.14	0.14	0.14	Width of the CPW's gap
L_T	3.64	**1.64**	1.64	1.64	Tapering length in the transition region
W_T	10.2	10.2	**9.2 A**	**8.5 B**	Upper tapering in the transition region
L_{R1}	4.33	4.33	4.33	4.33	Resonator length in the radiating region
L_{R2}	4.335	4.335	**1.835 B**	4.335 **A**	Resonator length in the matched radiating region
W_R	10.5	10.5	10.5	10.5	Resonator width in the radiating region
W_C	7	7	7	**7.2 C**	Circle's separation width
R	2.5	2.5	2.5	2.5	Radius of the top circle area
Bandwidth	4-14GHz	5-25GHz	6.5-45GHz	5-150GHz	Bandwidth enhancement

Table 1. Parameters of the prototypes (all dimensions are in mm), the alphabetical order A, B, C indicates the priority-order of parameters in the SVO process.

5. Design and Fabrication

5.1 Design

All prototypes depicted in Fig. 4, with their design dimensions listed in table.1, have been fabricated on Duroid RT 5880 high frequency laminate with substrate height h=0.787mm, copper cladding thickness t=17µm, relative dielectric constant ε_r=2.2, electric and magnetic loss tangents are given by tan δ_E=0.0027 and tan δ_H=0, respectively. The foremost reason of choosing this material is that it could relatively afford SWB frequency range up to 77 GHz (Huang et al., 2008, p.64). Other reasons are assessments related to temperature, moisture, corrosion and stability, which were investigated in details by (Brown et al., 1980).

5.2 Feed Elongation

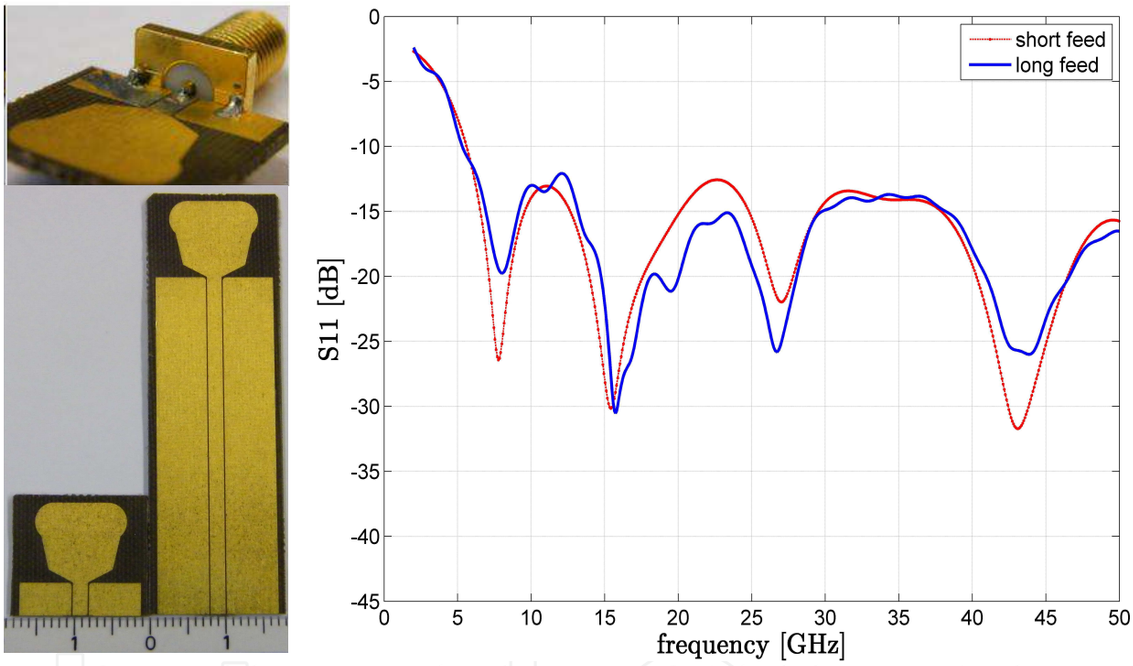

Fig. 6. Conceptual demonstration for advocating of CPW feed elongation, a) radiator with SMA connector, b) radiators with short and elongated feed, b) simulated reflection coefficient magnitudes of antenna with short and long feed.

Since the dimension of the SMA connector's flange is considerably large in comparison with the antenna dimension (see Fig. 6a), this comparable size exerts a huge impact on the antenna's electromagnetic-properties in particularly to the transmission, scattering and radiation mechanism. In order to reduce this obstruction and to measure the antenna's scattering parameters and radiation patterns adequately, it is necessary to elongate the antenna as show in Fig. 6b. To back up the advocating of this elongation, we exploited the facts that the co planar waveguide has negligible radiation, low-loss and constant effective dielectric constant in rather wide range of application from DC to above 50GHz. we decided to elongate the CPW feed L_F to 40mm, and carried out numerical simulations of the same SWB radiators with short and long feed. The magnitudes of the reflection coefficient are

compared and plotted in Fig. 6c. As expected, the numerical results exposed a negligible differences as theoretically has predicted (Simons, 2001, p.240). Note that these theoretical properties (negligible radiation and low-loss) were also experimentally consolidated by (Tanyer et al, op cit.).

6. Measurements

The prototype 4 is measured with the Agilent E8364B PNA vector network analyzer, the electronic calibration kit N4693A 2-port ECal-module was used for full-range calibration of the PNA (50GHz).

6.1 Reflection Coefficient

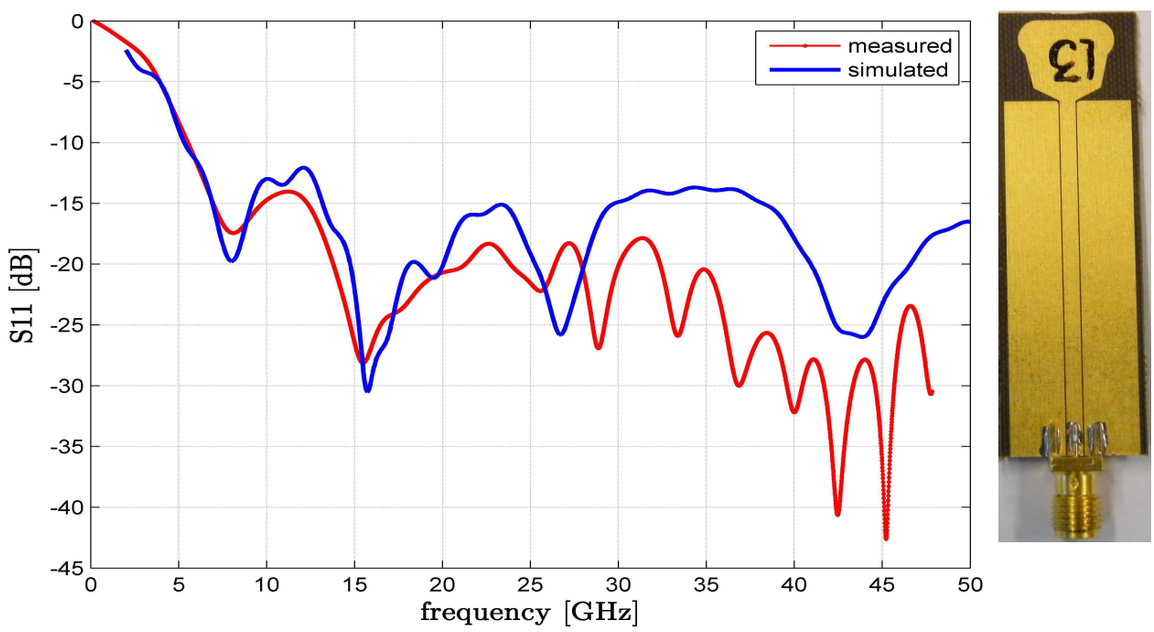

Fig. 7. SWB-performance: simulated and measured results.

The reflection coefficient magnitude of prototype 4 is measured and shown in fig. 7, the measurement agreed well with predicted value. Small deviation as frequency higher than 26 GHz, this defect is inherently caused by the failure of the 3.5mm SMA-connector, whose HF-range is cataloged as 18GHz max. The result indicated that the prototype 4 is a SWB-radiator because its measured ratio-bandwidth B_R is certainly greater than 10:1.

6.2 Far-field Radiation patterns

The far field radiation patterns are measured in the Delft University Chamber for Antenna Test (DUCAT); the anechoic chamber DUCAT (Fig. 8a) is fully screened, its walls, floor and ceiling are shielded with quality copper plate of 0.4 mm thick. All these aimed to create a Faraday cage of internal dimension of 6 x 3.5 x 3.5 m^3, which will prevent any external signal from entering the chamber and interfering with the measurements. The shielding of the

chamber is for frequencies above 2 GHz up to 18 GHz at least 120 dB all around (Ligthart, 2006). All sides are covered with Pressey PFT-18 and PFT-6 absorbers for the small walls and long walls, respectively. It is found that one side reflects less than -36 dB. All these measures were taken together in order to provide sufficient shielding from other radiation coming from high power marine radars in the nearby areas.

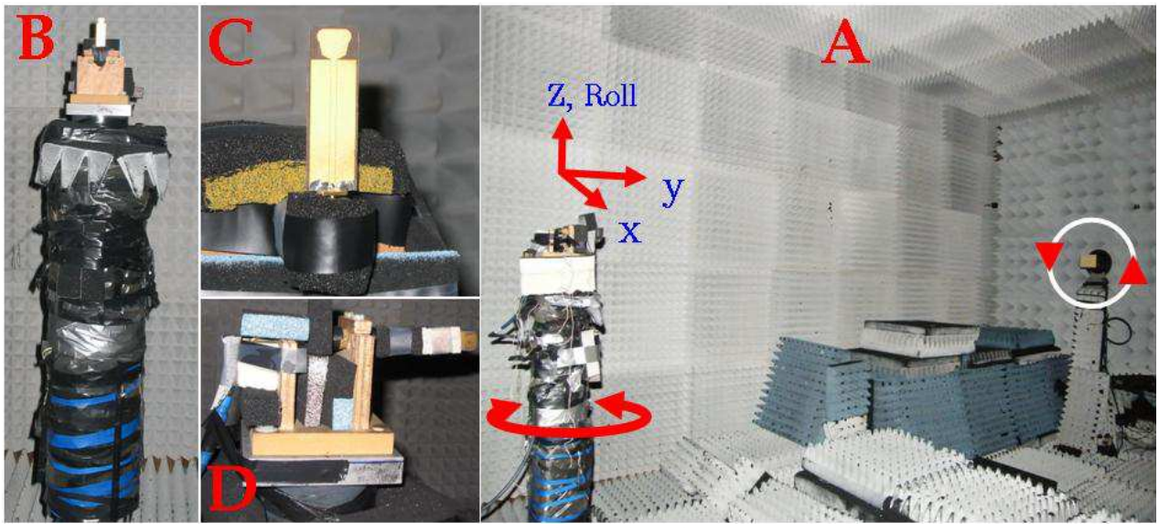

Fig. 8. Patterns measurement set up: a) anechoic chamber DUCAT, b) AUT on the rotatable column, c) Vertical configuration and d) Horizontal configuration.

TX: Single polarization standard horn is used as transmitter, which can rotate in yaw-y-direction to provide V, H polarizations and all possible slant polarizations. The choice of the single polarization horn above the dual polarization one as calibrator is two-folds: 1) keeps the unwanted cross-polarization to the lowest possible level, 2) and also voids the phase center interference and keeps the phase center deviation to the lowest level.
RX: Prototype 4 is put as antenna under test (AUT) on the roll-z-rotatable column (Fig. 8b). For the measurements of polarimetric components (VV, HV, VH, HH, the first letter denotes transmission's polarization state, the second is for the reception), two measurement setups are configured, the 1st is the vertical reception setup (VRS, Fig. 8c) for VV, VH and the 2nd is the horizontal reception setup (HRS, Fig. 8d) for HH, HV. Combination of the two setups and the TX's two polarizations provide full polarimetric patterns of the AUT.
Calibration: the HF-ranges of the Sucoflex-cable, T-adapters and connectors used in this measurement set up all cataloged as 18GHz max, owing to this limitation, we calibrated the PNA with Agilent N4691B cal-kit (1-26GHz).

6.2.1 Co-polar VV radiation patterns

The VV co-polar patterns are acquired with the VRS configuration in which TX-polarization is zenith-oriented. Fig. 9 showed the measured patterns in full calibrated range (§6.2). As predicted, the patterns were symmetrical- and omni-directional in the equipments' dynamic range. Fig. 10 shows the measured VV co-polar patterns for the in-band range (7-15GHz, 1GHz increment). The patterns consolidated the symmetrical receiving/transmitting mechanism of the AUT. Also observed is that all EIRP are less than -42dBm.

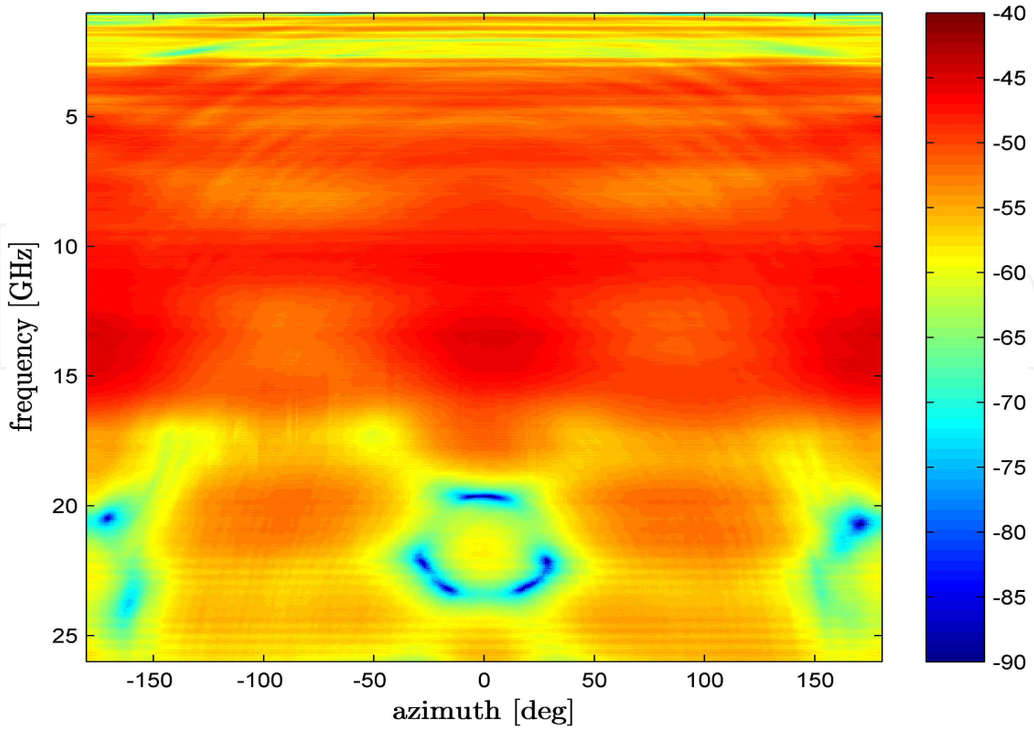

Fig. 9. Full-band VV co-polar measured patterns; RX: VRS; TX: zenithally oriented.

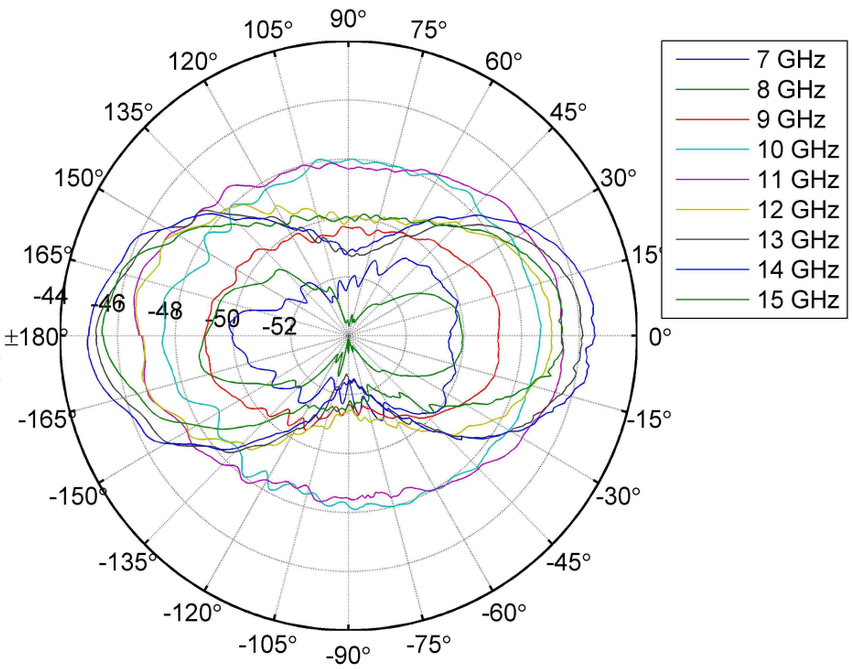

Fig. 10. In-band VV co-polar measured patterns; RX: VRS; Tx: zenithally oriented.

6.2.2 Cx-polar HV radiation patterns

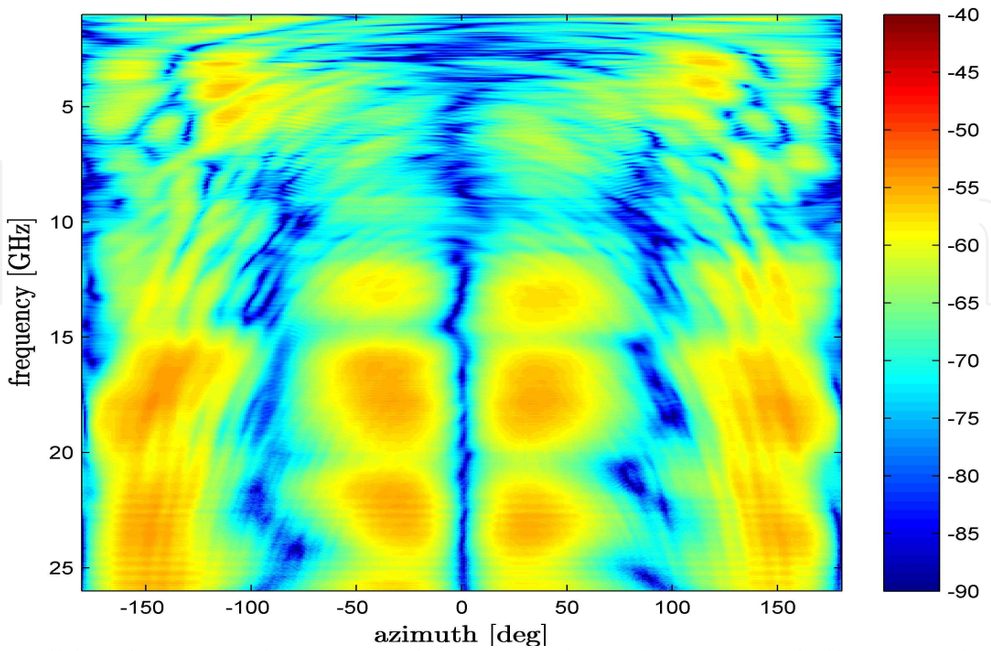

Fig. 11. Full-band HV cx-polar measured patterns; RX: VRS; Tx: azimuthally oriented.

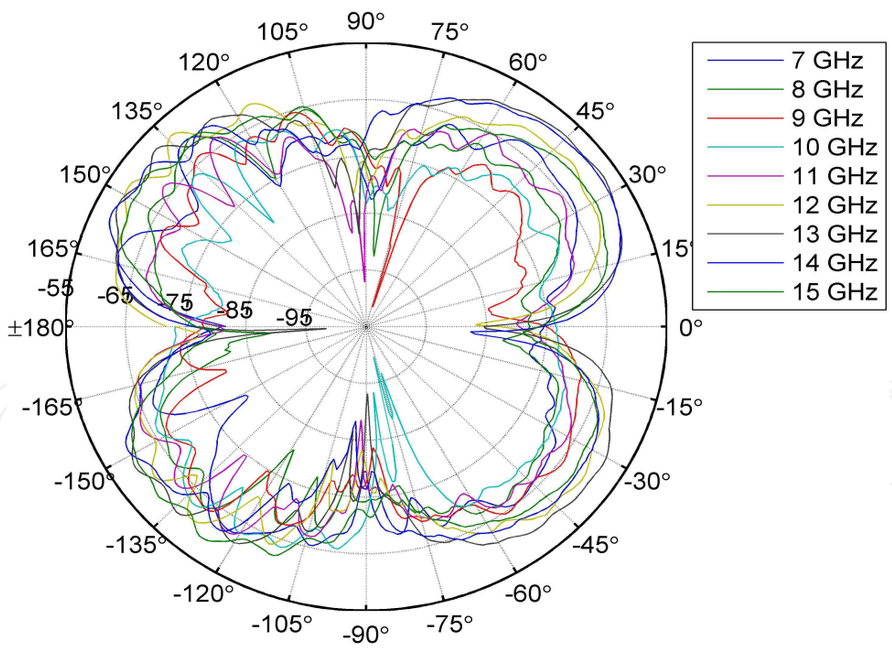

Fig. 12. In-band HV cx-polar measured patterns; RX: VRS; TX: azimuthally oriented.

The HV cx-polar patterns are obtained with the VRS configuration in which TX-polarization in Fig. 8a is 90^0-rotated. Plotted in Fig. 11 are the HV cx-polar patterns. As expected, perfect symmetrical and repeatable patterns can be observed in full-calibrated range (1-26GHz). Fig. 12 showed the measured HV cx-polar patterns for the in-band range (7-15GHz, 1GHz

increment). The patterns consolidated the repeatable symmetrical receiving/transmitting mechanism of the prototype 4. Also observed is that all EIRP are less than -65dBm, this revealed that a greater than -20dBm XPD is obtained. Note, in the yoz−plane, theoretically no cx-polar components are expected as all cross polar components cancel each other in the $0^0 — 180^0$ and $-90^0 — 90^0$ direction. In a real case scenario, some cx-polar components are observed, their level being, nonetheless, extremely low (~ -90dBm)

6.2.3 Co-polarized HH radiation patterns

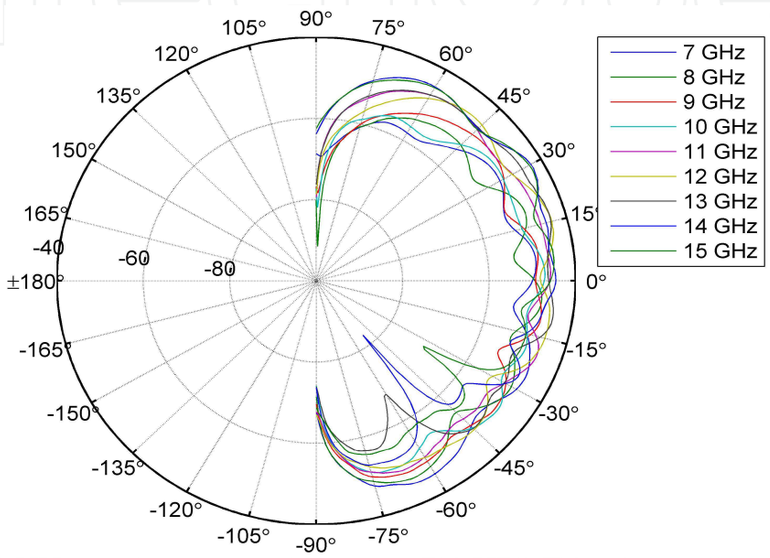

Fig. 13. In-band HH co-polar measured patterns; RX: HRS; TX: azimuthally oriented.

6.2.4 Cx-polarized VH radiation patterns

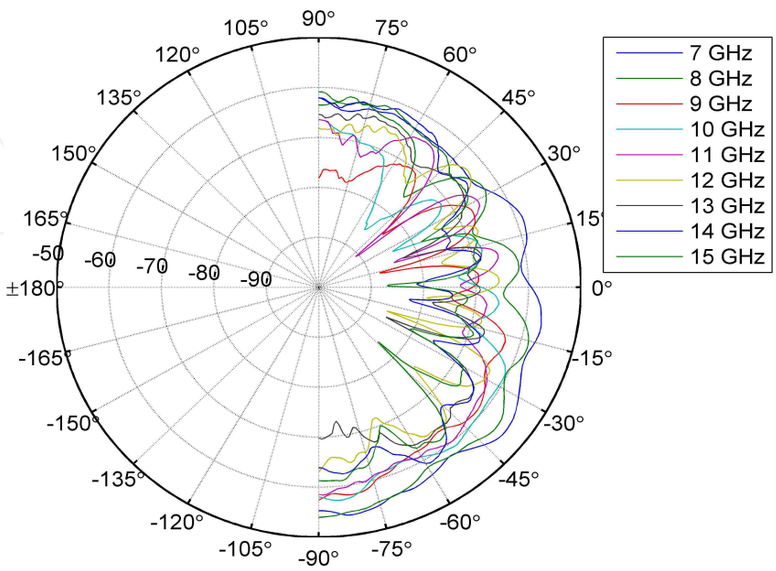

Fig. 14. In-band VH cx-polar measured patterns; RX: HRS; TX: zenithally oriented.

The co-polar (HH) and cx-polar (VH) radiation patterns can be acquired by the HRS with two polarization states of the TX, respectively. However, due to the mounting of the antenna (shown in Fig. 8d) it was not possible to measure the backside of the antenna, thus for the only half of the co-polar and cx-polar patterns were measured. Owing to the frequency limitations of used components (cables, adapters, connectors, absorbents), the DUCAT anechoic chamber specifications (Ligthart, 2006, op. cit.) and the WISE desired band the in-band range is chosen from 7-15GHz.
Fig. 13 showed the measured co-polar HH in-band radiation patterns. The patterns are symmetrical and repeatable with all EIRP less than -42dBm. The measured in-band cx-polar patterns for the VH configuration are plotted in Fig. 14, all peak powers have the EIRP in the order of -60dBm. The XPD of between HH and VH of the HRS displays the same discrimination dynamic as that of VV and HV of the VRS.

6.3 Time Domain Measurements

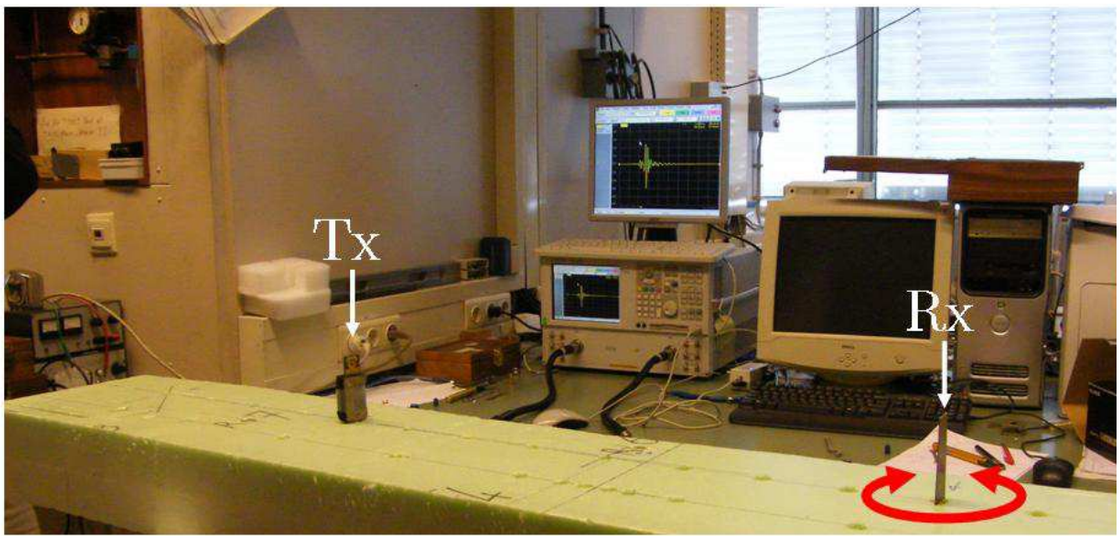

Fig. 15. Time domain measurement setups, equipment: Agilent VNA E8364B; Calibration kit: Agilent N4691B, calibrated method: 2-port 3.5 mm, TRL (SOLT), 300 KHz – 26 GHz

Fig. 15 shows the time domain set up for measurement and evaluation of: 1) pulse deformation, 2) the omni-radiation characteristics of the AUT. The same prototype 4 are used for TX (left) and RX (right), they stand on a horizontal foam bar which situated 1.20m above the floor.

6.3.1 Pulse Measurements

Pulse spreading and deformation: Fig. 16a shows the time-synchronization between the calculated transmit pulse (CTS) and the measured receive pulse (MRP) (for comparison, the CTS has been normalized, time-shifted and compared with the MRP), qualitative inspection shows that the synchronization-timing between transmitted and received pulses is very good, there is no pulse spreading took place, these measured features proved that the device is suitable for accurate ranging/sensing-applications, the small deviation at the beginning of

the received pulse is due to RF-leakage (Agilent, AN1287-12, p.38), and at the end of the received pulse are from environments and late-time returns (Agilent, ibid., p.38), Note that the measurements are carried out in true EM-polluted environment as shows in fig. 15, and no gating applied).

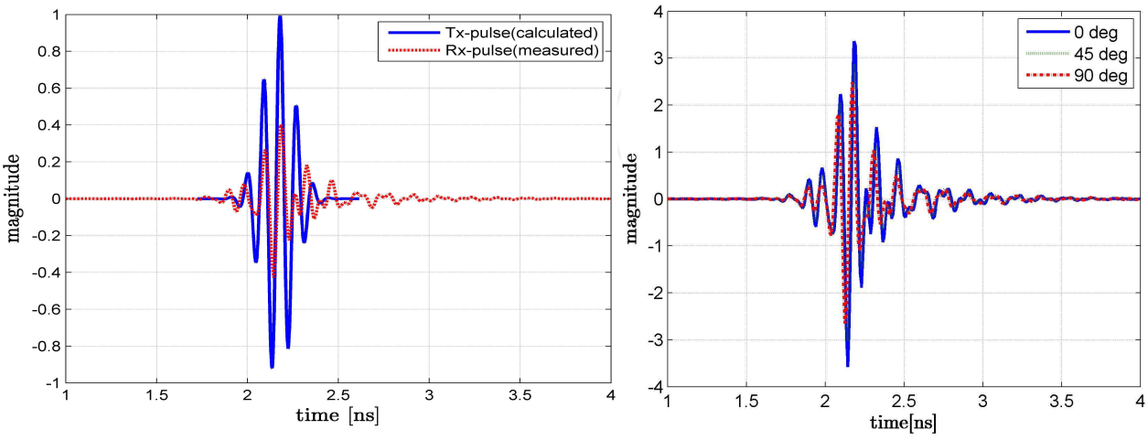

Fig. 16. co-polar transmission results of VRS-configuration; a) face-to-face: calculated vs. measured; b) oblique facing: measured results with RX 0-, 45- and 90-degree rotated.

Omni-radiation characteristics: To correctly evaluate the omni-directional property of the AUT, both quantitative characteristics (spatial) and qualitative characteristics (temporal) are carried out, the spatial-properties of prototype 4 are already tested and evaluated in frequency-domain (as depicted in fig. 9), and only the temporal-characteristic is left to be evaluated. To evaluated temporal-omni-radiation characteristics, three principal cuts are sufficiently represent the temporal-omni-radiation characteristics of the AUT in the time domain. Due to the editorial limitation, we report here only the most representative case (omni-directional in the azimuthal plane, i.e. co-polar VRS, which represents the most of all realistic reception scenarios). Fig. 16b shows three MRPs of the measurement configuration pictured in Fig. 15 with RX 0^0, 45^0, and 90^0 rotated. The results show a perfectly identical in timing, there is no time–deviation or spreading detected between the three cases. Furthermore, although the radiator is planar, it still exhibits a remarkable azimuth-independent property of 3D-symmetric radiators (for the 90^0 configuration, the projection of the receiving aperture vanished, however the prototype still able to receive 90% power as compare to the face-to-face case), this TD-measured results pertained the omni-directional property of the radiator, and this is also in agreement with, and as well consolidate the validity of the measured results carried out in the FD.

6.3.2 Transmission Amplitude Dispersion

To evaluate the amplitude spectral dispersion of the prototype 4, the measured time-domain transmission scattering coefficients of the three co-polar configurations (0^0, 45^0, and 90^0 configurations displayed in figure 15) were Fourier-transformed in to frequency domain. The measured magnitudes are plotted in fig. 17a, the measured results show a smooth and flat amplitude distribution in the designated band, and all are lower than -42dBm.

6.3.3 Transmission Phase Delay and Group delay

The measured phase responses of the transmission parameter for the three co-polar configurations are plotted in Fig. 17b. In narrowband technology, the phase delay defined as $\tau_P = -\theta/\omega$, is a metric for judging the quality of the transmission is the phase delay between the input and output signals of the system at a given frequency. In wideband technology, however, group delay is a more precise and useful measure of phase linearity of the phase response (Chen, 2007). The transmission group delays for the three above-mentioned configurations are plotted in Fig. 17c. The plots show an excellent and negligible group delays in the order of sub-nanosecond, this is no surprise because the phase responses of the prototype are almost linear (fig. 17b), thus the group delay, which is defined as the slope of the phase with respect to frequency $\tau_G = -d\theta/d\omega$, resulted accordingly. Note: although the group delay (fig. 17c) is mathematically defined as a constituent directly related to the phase, but it was impossible to visually observe directly from the phase plot (fig. 17b), but well from the magnitude plot (fig. 17a).

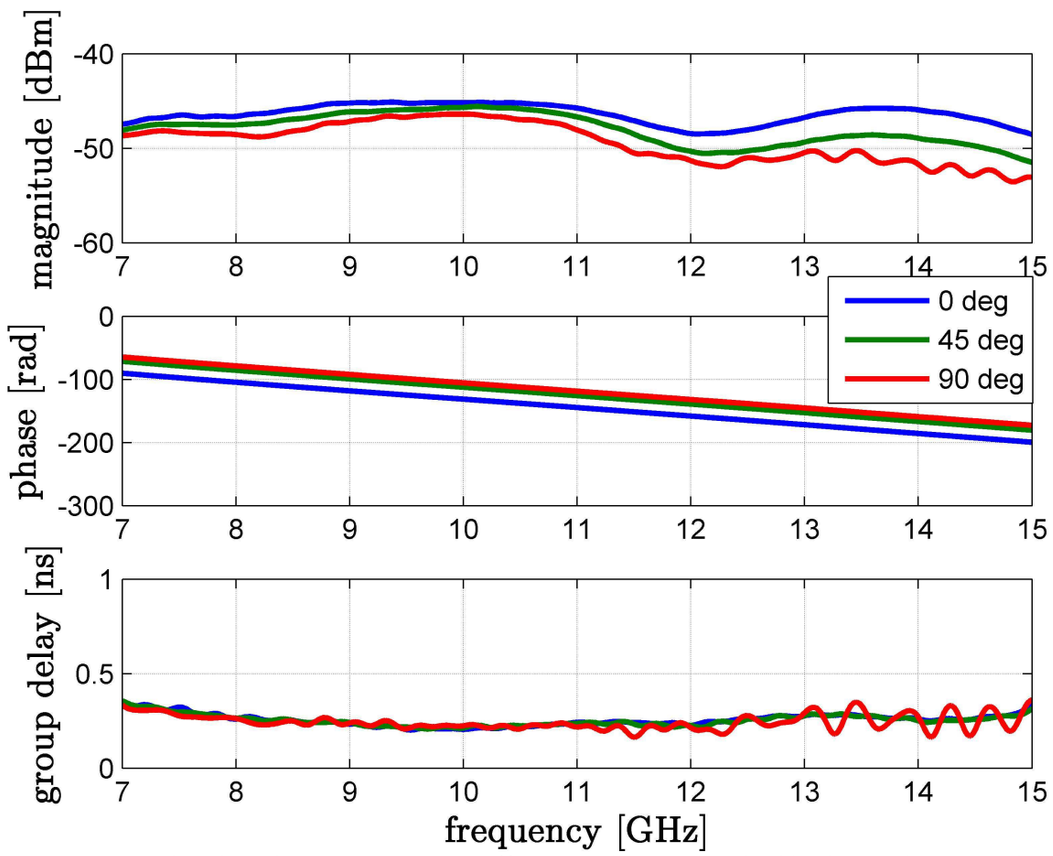

Fig. 17. Measured in-band transmission coefficients a) magnitude, b) phase, c) group delay

7. Acknowledgements

The research reported in this work was effectuated with in the frame of the "Wise Band Sparse Element Array Antennas" WiSE project, a scientific undergone financed by the Dutch

Technology Foundation (Stichting Technische Wetenschapen – STW). This support is hereby gratefully acknowledged.

8. Conclusions

The intent message of this report is not the mathematical formulation, nor the numerical aspects related to the design of proposed prototypes, but focusing on the concept, the design methodology and the pragmatic simplification of MVO process in to a SVO one.
Distinct concepts and definitions are defused and corrected. An SWB-antenna topology with simplest structure is proposed. The single layer topology paved the way for the creating of the obtained SWB antenna architecture. The antenna architecture supported, in turn, the FSD. The introduced design methodology and conceptual concept are consolidated by the developed prototypes.
The antenna architecture provides powerful isolated-parameters to control the antenna characteristics, such as resonance-shifting, resonance matching, bandwidth broadening, diffraction reduction, and SWB pattern maintaining.
The FSD approach is introduced to obtain the required performance, whilst keeping the overall dimension of the radiator fixed, the separated sections provide engineering insights, and can be designed or optimized almost independently.
Parameter order and SVO methodology are elaborated in details, the priority and role of separable parameters are identified, and so, instead of multivariable-optimization, the optimization process can be accelerated by carry out sequence of SVOs. The proposed design, optimization procedure can possibly be used as a gauging-process for designing or optimizing similar SWB structures.
Although the prototype 4 comprised a simplest structure and shape, however superior SWB impedance bandwidth is obtained and stable SWB-patterns are uniquely preserved.
This structure, although, can be modified to obtain huge frequency bandwidth, but cannot be one-size-fit-all for gain-size requirement. However, the architecture is flexible enough for scaling up/down its dimensions to match customer's gain-size requirement.
SWB prototype is designed, fabricated and evaluated for the super wideband impasse, and could possibly used as an alternative radiator for the sub-millimeter-wave regime.
Performances of the prototype are tested and evaluated. Good agreements between numerical predictions and measurements are obtained.
The SWB-prototype has been fabricated years ago but not published elsewhere; due to editorial limits, we exclusively report here only the design methodology and conceptual approach; detailed mathematical formulation and numerical aspects related to this SWB prototype will be published in another occurrence.

9. References

Agilent technologies (2007). Time Domain Analysis Using a Network Analyzer, Application Note 1287-12, 2007.

Al Sharkawy, M. H., Eldek, A. A., Elsherbeni, A. Z., and Smith, C. E. (2004). Design of wideband printed monopole antenna using WIPL-D". 20th *Annual Review of Progress in Applied Computational Electromagnetics*, NY, Syracuse, USA, Apr. 2004.

Balanis, C. A. (1997). *Antenna theory analysis and design*, John Wiley & Sons, Inc, second edition, New York, 1997.

Belrose, J. S. (1995). Fessenden and Marconi: Their Differing Technologies and Transatlantic Experiments During the First Decade of this Century, International *conference on 100 years of Radio*, 5-7 Sept. 1995.

Brodsky, I. (2008). How Reginald Fessenden Put Wireless on the Right Technological Footing, *Proceedings of the Global Communications Conference*, GLOBECOM 2008, New Orleans, LA, USA, 30 Nov.-4 Dec. 2008. pp.3577-81.

Brown, D., Fiscus, T. E, Meierbachtol, C. J (1980). Results of a study using RT 5880 material for a missile radome, In: *Symposium on Electromagnetic Windows*, 15th, Atlanta, GA, June 18-20, Proceeding (A82-2645, 11-32), Georgia Institute of Technology, p.7-12.

Chen Z.N. (2007). Antenna Elements for Impulse Radio, In: *Ultra-wideband Antennas and Propagation for Communications, Radar and Imaging*, Allen B. et al. (Ed.), John Wiley & Sons, 2007.

FCC (2002). Federal Communications Commission, FCC 02-48, ET-Docket 98-153, "*First Report and Order*", Apr. 2002.

FCC (2004), Federal Communications Commission, FCC 04-285, ET-Docket 98-153, "*Second Report and Order and Second Memorandum Opinion and Order*", Dec. 2004.

Huang, Y. & Boyle, K. (2008). *Antennas from Theory to Practice*, John Willey and Sons, Singapore, 2008, pp.64.

IEEE STD 145-1983. *IEEE Standard Definitions of Terms for Antennas*, New York, IEEE Press, 1983, pp.11-16.

Karoui, M. S., Ghariani, H., Samet, M., Ramadi, M., Pedriau, R. (2010). Bandwidth Enhancement of the Square Rectangular Patch Antenna for Biotelemetry applications, *International journal of information systems and telecommunication engineering*, v.1, 2010, iss.1, pp.12-18.

Kraus, J. D. (1985). Antennas since Hertz and Marconi, *IEEE Trans*. AP-33, No. 2, Feb.1985, pp.131-137.

Kshetrimayum, R. S., Pillalamarri, R. (2008). Novel UWB printed monopole antenna with triangular tapered feed lines, *IEICE Electronics express*, vol.5, No. 8, pp. 242-247.

Ligthart, LP (2006). Antennas and propagation measurement techniques for UWB radio, *Wireless personal communications*, 37(3-4), pp.329-360.

Massey, P. (2007). Planar Dipole-like for Consumer Products, In: *Ultra-wideband Antennas and Propagation for Communications, Radar and Imaging*, Allen, B. et al., John Wiley & Sons, West Sussex, England, 2007, pp.163-196.

Molisch, A. F., (2007). Introduction to UWB signals and system, In: *Ultra-wideband antennas and propagation for communications, radar and ranging,* Allen, B. et al., (Ed.), pp.1-17, John Willey and sons, West Sussex, England.

Rahayu, H., Rahman, T. A., Ngah, R., Hall, P. S. (2008). Slotted ultra wideband antenna for bandwidth enhancement, 2008, *Loughborough Antennas & Propagation Conference* 17-18, Mar. 2008, Loughborough, UK.

Rahim, M. K. A. & Gardner, P. (2004). The design of nine element quasi microstrip log periodic antenna, *RF and microwave conference*, 2004. RFM 2004, 5-6 Oct. 2004, Selangor, Malaysia, pp.132–135.

Razavi, B. et al. (2005). A UWB CMOS Tranceiver, *IEEE journal of solid-state circuit*, vol.40, no.12, dec. 2005, pp.2555-2562.

Rmili, H. & Floc'h, J. M. (2008). Design and analysis of wideband double-sided printed spiral dipole antenna with capacitive coupling, *Microwave and optical technology letters,* Vol. 50, No.5, pp. 312-1317.

Schantz, H. G and Barnes, M. (2003). UWB magnetic antenna, *IEEE International Symposium on Antennas and Propagation Digest*, 3, 2003, pp.604-607.

Schantz, H. G. (2004). A brief history of UWB antennas, *IEEE Aerospace and Electronic Systems Magazine*, vol .19(4), pp.22-26, 2004.

Simons, R. N. (2001). *Coplanar Waveguide Circuits, Components, and Systems*, John Wiley & Sons, New York, 2001.

Tanyer-Tigrek, F. M, Tran, D., Lager, I. E., Ligthart, L. P. (2009a). CPW-fed Quasi–Magnetic Printed Antenna for Ultra-Wideband Application, *IEEE Antennas and Propagation Magazine*, Vol.51, No.2, April 2009, 1, pp.61-70.

_____, (2009b). Over 150% bandwidth, quasi-magnetic printed antennas, *Antennas and Prop. Society International Symposium,* AP-S, 2009.

_____, (2010). *Printed antenna elements with attested ultra wideband array capability*, dissertation, ISBN-978-90-9024664-2, 2010, p.113-135.

Thor, R. C. (1962). A Large Time-Bandwidth Product Pulse-Compression Technique, *IRE Transaction on military electronics*, Vol. MIl-6, No.2, Apr. 1962, pp.169-173.

Tourette, S., Fortino, N., Kossiavas, G. (2006). Compact UWB printed antennas for low frequency applications matched to different transmission lines, *Microwave and optical technology letters*, Vol. 49, No.6, pp.1282-1287.

Tran, D., Tanyer-Tigrek, F. M., Vorobyov, A., Lager, I. E. & Ligthart, L. P. (2007). A Novel CPW-fed Optimized UWB printed Antenna, In: *Proceedings of the 10th European conference on wireless technology,* pp.40-43, Munich, Germany, October 8-10, 2007, Horizon House Publications Ltd, London.

Tran, D. P., Coman, C. I., Tanyer-Tigrek, F. M., Szilagyi, A., Simeoni, M., Lager, I. E., Ligthart, L. P. & van Genderen, P.(2010).The relativity of bandwidth – the pursuit of truly ultra wideband radiators, In: *Antennas for Ubiquitous Radio Services in a Wireless Information Society*, Lager, I. E (Ed.), pp.55-74, IOS Press, 2010, Amsterdam.

Wilson, J. M (2002). Ultra-wideband a disruptive RF technology?, Intel Research and Development, Version 1.3, Sept. 10, 2002.

Zhang, X., Wu, W., Yan, Z. H., Jiang, J. B. & Song, Y. (2009). Design of CPW-Fed monopole UWB antenna with a novel notched ground, *Microwave and optical technology letters*, Vol. 51, No.1, pp. 88-91.

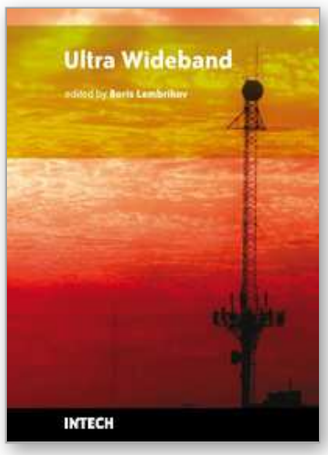

Ultra Wideband

Edited by Boris Lembrikov

ISBN 978-953-307-139-8

Hard cover, 458 pages

Publisher Sciyo

Published online 17, August, 2010

Published in print edition August, 2010

Ultra wideband technology is one of the most promising directions in the rapidly developing modern communications. Ultra wideband communication system applications include radars, wireless personal area networks, sensor networks, imaging systems and high precision positioning systems. Ultra wideband transmission is characterized by high data rate, availability of low-cost transceivers, low transmit power and low interference. The proposed book consisting of 19 chapters presents both the state-of-the-art and the latest achievements in ultra wideband communication system performance, design and components. The book is addressed to engineers and researchers who are interested in the wide range of topics related to ultra wideband communications.

InTech Europe
University Campus STeP Ri
Slavka Krautzeka 83/A
51000 Rijeka, Croatia
Phone: +385 (51) 770 447
Fax: +385 (51) 686 166
www.intechopen.com

InTech China
Unit 405, Office Block, Hotel Equatorial Shanghai
No.65, Yan An Road (West), Shanghai, 200040, China
中国上海市延安西路65号上海国际贵都大饭店办公楼405单元
Phone: +86-21-62489820
Fax: +86-21-62489821

IntechOpen